Original Article

Institution of MECHANICAL ENGINEERS
Journal of ENGINEERING IN MEDICINE

Proc IMechE Part H:
J Engineering in Medicine
2020, Vol. 234(7) 660–673

DOI: 10.1177/0954411920913374
journals.sagepub.com/home/pih
SAGE

Dynamic-joint-strength-based two-dimensional symmetric maximum weight-lifting simulation: Model development and validation

Ritwik Rakshit[1], Yujiang Xiang[2] and James Yang[1]

Abstract

This article presents an optimization formulation and experimental validation of a dynamic-joint-strength-based two-dimensional symmetric maximum weight-lifting simulation. Dynamic joint strength (the net moment capacity as a function of joint angle and angular velocity), as presented in the literature, is adopted in the optimization formulation to predict the symmetric maximum lifting weight and corresponding motion. Nineteen participants were recruited to perform a maximum-weight-box-lifting task in the laboratory, and kinetic and kinematic data including motion and ground reaction forces were collected using a motion capture system and force plates, respectively. For each individual, the predicted spine, shoulder, elbow, hip, knee, and ankle joint angles, as well as vertical and horizontal ground reaction force and box weight, were compared with the experimental data. Both root-mean-square error and Pearson's correlation coefficient (r) were used for the validation. The results show that the proposed two-dimensional optimization-based motion prediction formulation is able to accurately predict all joint angles, box weights, and vertical ground reaction forces, but not horizontal ground reaction forces.

Keywords

Lifting, dynamic joint strength, strength percentile, maximum weight, inverse-dynamics optimization, predictive dynamics, motion prediction, validation, manual material handling

Date received: 18 July 2019; accepted: 13 February 2020

Introduction

Lifting tasks are a necessary and important part of the construction and shipping industries. However, they can put workers at risk of serious injury and reduce revenue for businesses in the form of lost man-hours from sick leaves, and insurance and disability payouts. It is therefore desirable to have a model capable of predicting maximum safe lifting weight. The National Institute for Occupational Safety and Health (NIOSH) lifting equation is a simplistic method to estimate the maximum load that healthy employees can lift over the course of an 8-h shift without increasing their risk of lower back musculoskeletal disorders.[1] However, it must be considered that biological joints are fundamentally different from robotic ones in the sense that their torque capacity changes with joint angle, angular velocity, strength percentile, and time.[2–7] In muscle space, the net moment capacity depends on the crossing muscles' moment-generating capacity which further depends on the muscles' moment arms, force–length, and force–velocity properties. These muscle properties change with the joint angles and angular velocities. Therefore, dynamic joint strength is a three-dimensional (3D) function of joint angle and angular velocity. Since joint angle and angular velocity are time-dependent functions for a given task, dynamic joint strength is also an implicit function of time. Based on data from literature, a model incorporating dynamic joint strengths (torque limits) will therefore be more accurate than one using static strengths. It is the

[1]Human-Centric Design Research Lab, Department of Mechanical Engineering, Texas Tech University, Lubbock, TX, USA
[2]School of Mechanical and Aerospace Engineering, Oklahoma State University, Stillwater, OK, USA

Corresponding author:
Yujiang Xiang, School of Mechanical and Aerospace Engineering, Oklahoma State University, Stillwater, OK 74078, USA.
Email: yujiang.xiang@okstate.edu

objective of this work to demonstrate and experimentally validate such a model.

Compared to experimental methods,[8] predictive methods are more powerful in cause-and-effect studies. Human predictive simulation methods available in the literature can be roughly divided into five categories: forward-dynamics simulations,[9] inverse-dynamics simulations,[10,11] collocation methods,[12,13] control-based methods,[14] and mixed-formulation methods.[15] Each of these methods have their individual advantages and limitations in terms of the computational time required, accuracy, robustness, and the ability to handle different models.[16] Ayoub,[17] Hsiang and Ayoub,[18] and Aghazadeh and Ayoub[19] conducted pioneering research into lifting simulation using the optimization approach. Chang et al.[20] used an inverse-dynamics optimization approach to predict sagittal plane lifting motion by minimizing joint torque squared cost function. Intermediate postures were used as constraints in the optimization formulation in Chang et al.[21] However, the dynamic joint strength was not considered in these optimization formulations. Gündogdu et al.[22] considered dynamic joint strength limits in the optimization formulation for two-dimensional (2D) lifting simulation. The effects of lifting time, box weight, and lifting strategy were investigated. However, experimental validation was not conducted.

In this study, inverse-dynamics optimization is adopted for a 2D symmetric lifting simulation considering dynamic strength. This method can not only predict motion but is also more computationally efficient because the equations of motion (EOM) are directly evaluated from inverse dynamics in each optimization iteration.[23] In addition, there are various methods in the literature that predict lifting motion such as the time finite element method,[24] the forward-dynamics optimization method,[25] and the inverse-dynamics optimization method.[20,21,26] However, only a few studies have considered dynamic strength for lifting motion prediction.[22] By considering dynamic strength, the symmetric-maximum-lifting weight can be predicted for injury prevention in joint space. It is noted that there are other injury criteria in muscle space that necessitate the use of a musculoskeletal model. One example of muscle injury is skeletal muscle strain injury during lifting.[27] The other criterion could be lumbar spine compression stress.[28]

The objective of this article is to develop a dynamic-joint-strength-based maximum weight-lifting simulation and to conduct experiments to validate the proposed model.

Method

Human simulation model

The 2D model has $n = 10$ degrees of freedom (DOFs): three global DOFs (q_1, q_2, q_3) and seven physical joints ($q_4, \ldots, q_{10}$), as shown in Figure 1. The global DOFs include two translations (q_1, q_2) and one rotation (q_3) which move the pelvis to the current position in inertial Cartesian coordinates. Collectively, the DOFs are defined as $\mathbf{q} = [q_1, \ldots, q_{10}]^{\mathrm{T}}$. Because the model is symmetric in the sagittal plane, only one set of shoulder (q_5), elbow (q_6), hip (q_7), knee (q_8), ankle (q_9), and metatarsophalangeal joints (q_{10}) is considered in the model. In addition, for these symmetric joints, the joint strength, the corresponding link mass, and the moment of inertia are doubled. The Denavit–Hartenberg method[29] is used to build the skeletal model, and recursive Lagrangian dynamics are used to set up EOM for the model as follows.[30]

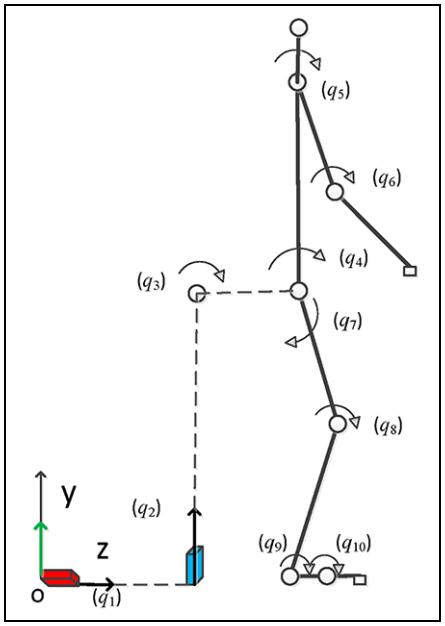

Figure 1. 2D human model.

Forward recursive kinematics

$$\mathbf{A}_i = \mathbf{A}_{i-1}\mathbf{T}_i \tag{1}$$

$$\mathbf{B}_i = \mathbf{B}_{i-1}\mathbf{T}_i + \mathbf{A}_{i-1}\frac{\partial \mathbf{T}_i}{\partial q_i}\dot{q}_i \tag{2}$$

$$\mathbf{C}_i = \mathbf{C}_{i-1}\mathbf{T}_i + 2\mathbf{B}_{i-1}\frac{\partial \mathbf{T}_i}{\partial q_i}\dot{q}_i + \mathbf{A}_{i-1}\frac{\partial^2 \mathbf{T}_i}{\partial q_i^2}\dot{q}_i^2 + \mathbf{A}_{i-1}\frac{\partial \mathbf{T}_i}{\partial q_i}\ddot{q}_i \tag{3}$$

where q_i is the joint angle variable; $\mathbf{T}_i$ is the 4×4 Denavit–Hartenberg link transformation matrix from the $(i-1)$th link frame to the ith link frame; $\mathbf{A}_i$, $\mathbf{B}_i$, and $\mathbf{C}_i$, are the global recursive kinematics

position, velocity, and acceleration matrices, respectively; and $\mathbf{A}_0 = [\mathbf{I}]$ and $\mathbf{B}_0 = \mathbf{C}_0 = [\mathbf{0}]$.

Backward recursive dynamics

$$\tau_i = tr\left(\frac{\partial \mathrm{A}_i}{\partial q_i}\mathbf{D}_i\right) - \mathbf{g}^{\mathrm{T}}\frac{\partial \mathbf{A}_i}{\partial q_i}\mathbf{E}_i - \mathbf{f}_k^{\mathrm{T}}\frac{\partial \mathbf{A}_i}{\partial q_i}\mathbf{F}_i - \mathbf{G}_i^{\mathrm{T}}\mathbf{A}_{i-1}\mathbf{z}_0 \tag{4}$$

$$\mathbf{D}_i = \mathbf{I}_i\mathbf{C}_i^{\mathrm{T}} + \mathbf{T}_{i+1}\mathbf{D}_{i+1} \tag{5}$$

$$\mathbf{E}_i = m_i\mathbf{r}_i + \mathbf{T}_{i+1}\mathbf{E}_{i+1} \tag{6}$$

$$\mathbf{F}_i = \mathbf{r}_k\delta_{ik} + \mathbf{T}_{i+1}\mathbf{F}_{i+1} \tag{7}$$

$$\mathbf{G}_i = \mathbf{h}_k\delta_{ik} + \mathbf{G}_{i+1} \tag{8}$$

where $tr(\cdot)$ is the trace of a matrix, $\mathbf{I}_i$ is the inertia matrix for link i, $\mathbf{D}_i$ is the recursive inertia-and-Coriolis matrix, $\mathbf{E}_i$ is the recursive vector for gravity torque calculation, $\mathbf{F}_i$ is the recursive vector for external force torque calculation, $\mathbf{G}_i$ is the recursive vector for external moment or torque calculation, $\mathbf{g}$ is the gravity vector, m_i is the mass of link i, $\mathbf{r}_i$ is the center of mass of link i, $\mathbf{f}_k = [\,0 \quad f_{ky} \quad f_{kz} \quad 0\,]^{\mathrm{T}}$ is the external force applied on link k, $\mathbf{r}_k$ is the position of the external force in the local frame k, $\mathbf{h}_k = [\,h_x \quad 0 \quad 0 \quad 0\,]^{\mathrm{T}}$ is the external moment applied on link k, $\mathbf{z}_0 = [\,0 \quad 0 \quad 1 \quad 0\,]^{\mathrm{T}}$ for a revolute joint, $\mathbf{z}_0 = [\,0 \quad 0 \quad 0 \quad 0\,]^{\mathrm{T}}$ for a prismatic joint, δ_{ik} is the Kronecker delta, and the starting conditions are $\mathbf{D}_{n+1} = [\mathbf{0}]$ and $\mathbf{E}_{n+1} = \mathbf{F}_{n+1} = \mathbf{G}_{n+1} = [\mathbf{0}]$.

Inverse-dynamics optimization formulation considering dynamic strength

For the inverse-dynamics optimization problem, the design variables are cubic B-spline control points of joint angle $\mathbf{q}_c$ and box weight W. The objective function f is the negative box weight which is to be minimized (maximizing the total weight)

$$f(W) = -W \tag{9}$$

The lifting optimization problem is subjected to the following constraints: joint angle limits, where $\mathbf{q}$ is the joint angle profile, and $\mathbf{q}^L$ and $\mathbf{q}^U$ are the lower and the upper bounds, respectively

$$\mathbf{q}^L \leqslant \mathbf{q}(t) \leqslant \mathbf{q}^U \tag{10}$$

Dynamic strength is considered in the simulation and is imposed as a set of joint torque limits, where the lower and the upper torque limits are functions of joint angle, angular velocity (v), strength percentile (z_score), and time (t): $\tau_i^L = \tau_i^L(q_i, v_i, z\_\text{score}, t)$ and $\tau_i^U = \tau_i^U(q_i, v_i, z\_\text{score}, t)$. These two functions are logistic regression equations obtained from isometric and isokinetic strength tests using dynamometers[4–6]

$$\tau^i_{\text{peak\_U}} = c_1 + c_2\frac{4e^{-(q_i-c_3)/c_4}}{\left[1+e^{-(q_i-c_3)/c_4}\right]^2} + c_5\frac{4e^{-(v_i-c_6)/c_7}}{\left[1+e^{-(v_i-c_6)/c_7}\right]^2} + c_8\frac{4e^{-(q_i-c_3)/c_4}}{\left[1+e^{-(q_i-c_3)/c_4}\right]^2}\frac{4e^{-(v_i-c_6)/c_7}}{\left[1+e^{-(v_i-c_6)/c_7}\right]^2} \tag{11}$$

$$\tau_i^U = z\_\text{score}\times\text{CV}^i_{\text{U}}\times\tau^i_{\text{peak}_{\text{U}}}(q_i, v_i, t) + \tau^i_{\text{peak}_{\text{U}}}(q_i, v_i, t) \tag{12}$$

$$\tau_i \leqslant \tau_i^U(q_i, v_i, z\_\text{score}, t), \quad i = 4, \ldots, n \tag{13}$$

where $c_1 - c_8$ are regression coefficients, e is the exponential function, $\tau^i_{\text{peak\_U}}$ is the peak upper torque value for the ith joint in the positive q_i direction as defined in Figure 1, and CV^i_{U} is the upper coefficient covariance for the ith joint.

Similarly, for the lower joint torque limit

$$\tau^i_{\text{peak\_L}} = d_1 + d_2\frac{4e^{-(q_i-d_3)/d_4}}{\left[1+e^{-(q_i-d_3)/d_4}\right]^2} + d_5\frac{4e^{-(v_i-d_6)/d_7}}{\left[1+e^{-(v_i-d_6)/d_7}\right]^2} + d_8\frac{4e^{-(q_i-d_3)/d_4}}{\left[1+e^{-(q_i-d_3)/d_4}\right]^2}\frac{4e^{-(v_i-d_6)/d_7}}{\left[1+e^{-(v_i-d_6)/d_7}\right]^2} \tag{14}$$

$$\tau_i^L = z\_\text{score}\times\text{CV}^i_{\text{L}}\times\tau^i_{\text{peak}_{\text{L}}}(q_i, v_i, t) + \tau^i_{\text{peak}_{\text{L}}}(q_i, v_i, t) \tag{15}$$

$$\tau_i \geqslant \tau_i^L(q_i, v_i, z\_\text{score}, t), \quad i = 4, \ldots, n \tag{16}$$

where $d_1 - d_8$ are regression coefficients, e is the exponential function, $\tau^i_{\text{peak\_L}}$ is the lower peak torque value for the ith joint in the negative q_i direction as defined in Figure 1, and CV^i_{L} is the lower coefficient covariance for the ith joint.

For dynamic joint strength constraints in equations (11)–(16), the coefficients $c_1 - c_8$, $d_1 - d_8$, and CV are obtained from experiments in the literature.[4–6] However, the participant-specific strength z_score is obtained from an enumeration process by solving an optimization problem which is formulated as follows: given maximum box weight, lifting time duration, and posture constraints from experimental data, minimize the sum of the squares of joint torques (the objective function) subjected to lifting-task-based constraints including strength limits and enumerate strength z_score until the optimization problem converges.[7] The participant-specific z_score thus obtained is the minimal strength percentile required to lift the corresponding maximum box weight. This z_score is used to build dynamic joint torque limits in equations (11)–(16).

Balance must be considered during the box-lifting process. This balance is a zero-moment-point (ZMP)

constraint. p_{ZMP} is the ZMP location, and FSR represents the foot-support region

$$p_{ZMP}(\mathbf{q},\ t) \in FSR \tag{17}$$

In addition, the feet are fixed on level ground. p_{foot} is the foot position calculated from the 2D skeletal model, and p^E_{foot} is the foot position measured from the experiment

$$p_{foot}(\mathbf{q},\ t) = p^E_{foot} \tag{18}$$

The initial and final box-grasping locations are derived from experimental data

$$p_{hand}(\mathbf{q},\ t) = p^E_{box}(t), \quad t = 0,\ T \tag{19}$$

where p_{hand} is the calculated hand position and p^E_{box} is the measured box-handle position.

Finally, the joint angle differences between the model and the experiment are constrained to a small range ($\varepsilon = 0.1$ rad) at the boundaries and to a larger range ($\varepsilon = 0.15$ rad) at 25%, 50%, and 75% of lifting duration. $\mathbf{q}^E$ is the experimental joint angle

$$\begin{aligned} &\left|q_i(t) - q^E_i(t)\right| \leqslant \varepsilon, \\ &t = 0,\ \frac{T}{4},\ \frac{T}{2},\ \frac{3T}{4},\ T;\ \ i = 4,\ \ldots,\ 10 \end{aligned} \tag{20}$$

where $t = [0,\ T/4,\ T/2,\ 3T/4,\ T]$, $t = [0,\ T/4,\ \ 3T/4,\ T]$, $t = [0,\ T/2,\ T]$, $t = [0,\ T]$ for 3, 2, 1, and 0 intermediate joint angle constraints, respectively. The intermediate joint angle constraint 3 is the default formulation, and 2, 1, and 0 intermediate constraints are studied for the purpose of drawing comparisons.

The ground reaction forces (GRF) are calculated from an inverse procedure based on joint kinematics, gravity, and external loads[11] during the optimization iteration. The total time T is obtained from experimental data.

Experimental data collection

Participants. A total of 23 male volunteers between 20 and 50 years of age were recruited for participation in the lab experiments. Capture data collected from four participants were found to be incomplete due to intermittently missing marker data during post-processing and therefore discarded. Finally, 19 participants were used for this study (age: 31 ± 11 years; height: 180.8 ± 6.2 cm; body mass: 82.17 ± 11.87 kg, all reported as mean ± standard deviation). The participants were required to have had no recent musculoskeletal disorders, to be able to perform the scripted task, and to not be on any medication that might impede their performance during the box-lifting task. The experimental procedures were approved by the Institutional Review Board of Texas Tech University, and all participants gave written informed consent.

Experimental protocol. 3D kinematic data were collected at 100 Hz using a Vicon Nexus motion capture system (Vicon, Oxford, UK). Five cameras were placed around the room, with one in each corner and one in the middle front of the room. A plug-in-gait model with added iliac crests,[31] yielding a total of 42 markers, was used for the marker protocol.[32] There were two force plates—one under each of the participants' feet—that collected GRF at 2000 Hz. The following anthropometric measurements were taken for each participant used for the plug-in-gait model during post-processing: height, weight, leg length, ankle width, knee width, wrist width, elbow width, shoulder offset, inter-ASIS distance, and waist circumference.[28,33]

For the lifting study, each participant was asked to psychophysically determine their maximum weight-lifting capability by gradually increasing the load (starting from a comfortable weight) until the participant requested to stop any further increase. The real maximum (lifting capacity) was not used in order to avoid injury during the experiment. Therefore, the maximum weight refers to maximum safe-lifting weight in this study. Once the weight was determined, the lifting study was initiated. The participant was asked to lift a box (65 cm × 35 cm × 15 cm) forward, symmetrically, in three trials, with a 5-min break after each. As the box did not have handles, it was placed in front of the participant on top of a 1-inch-tall weighted disk resting on the floor so that they could reach under the box to grab it with their fingers. They then lifted the box in a manner that felt the most comfortable and natural to them and set it down on a 1-m-tall table in front of them, as seen in Figure 2. All participants used the same table as there was only a small variation in their heights. Following the experiment, the data were processed in the Vicon Nexus motion capture software.

Data processing. All markers were labeled, and the data were smoothed and converted into a C3D file, which was then imported into Visual 3D (C-Motion, Inc., Germantown, MD, USA). A skeletal model, created following the marker protocol used in the experiments and consisting of 15 segments, was used to output coordinates and joint angles.

The experimentally measured heights and weights of each of the 19 usable participants were used to generate their body segments' lengths, centers of mass, and inertial properties using GEBOD™, a regression-based interactive utility.[34] The six joint angles (spine, shoulder, elbow, hip, knee, and ankle) and the box weight obtained from the experiments for each individual participant, in combination with the generated anthropometric data, were used to calculate the strength percentile (z_score) for each participant using the enumeration-based dynamic optimization algorithm

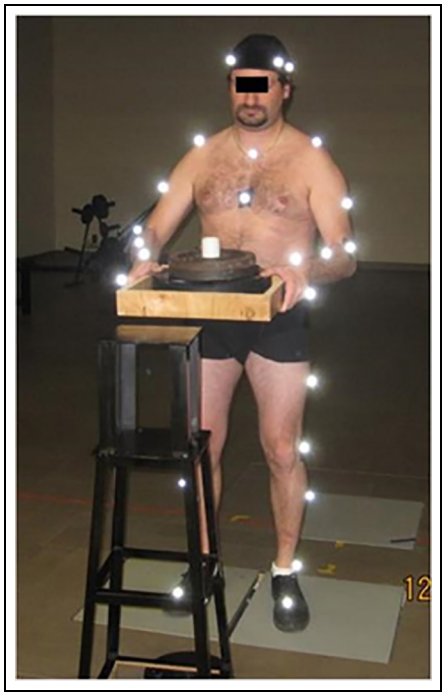

Figure 2. Maximum weight-lifting experiment.

described in section "Inverse-dynamics optimization formulation considering dynamic strength." Finally, the proposed 2D symmetric inverse-dynamics-based motion simulation was used to predict motions, GRF, and maximum box weights.

Results

In this study, we validate the proposed model in three different ways: (1) compare the simulation results with experimental data participant-by-participant, as each participant used a different maximum lifting strategy; (2) calculate the root-mean-square error (RMSE) between the predicted results and the experimental data; and (3) calculate Pearson's coefficient (r) between the simulation results and the experimental data. Furthermore, we have compared the results from different formulations such as dynamic strength limits, static strength limits, and NIOSH equation.

The eight parameters (spine, shoulder, elbow, hip, knee, and ankle angle profiles, and vertical and horizontal GRF) are plotted for Participants #15 and #9, as shown in Figures 3 and 4, respectively (the solid line denotes model simulation and the dashed line denotes experimental data). Note that the metatarsophalangeal joint angle was always zero during the lifting process because the foot did not move relative to the ground, and it was hence not plotted. Figure 5 shows stick-diagrams of lifting for all the participants.

Figures 6 and 7 depict the predicted joint torque profiles based on dynamic strength limits for Participants #15 and #9, respectively. Figure 8 depicts the predicted joint torque profiles for Participant #9 using static joint strength limits.

For Participants #15 and #9, all six predicted joint angles in Figures 3 and 4 follow the same trend as the experimental data. The predicted joint angles are also close to the experimental values (Pearson's r averaged across the six joints for Participants #15 and #9 are 0.98 and 0.99, respectively). The predicted vertical GRF shown in Figures 3(g) and 4(g) have similar magnitude to the experimental data, but the experimental GRF have a wavering nature to some extent—likely a result of the postural control that is always observable in experimental data. The experimental horizontal GRF shown in Figures 3(h) and 4(h), however, deviate to some extent from their corresponding prediction values at the initial stage of lifting. Participants usually initiate maximum weight lifting with a large acceleration. In addition, due to the large dimension of the box in the sagittal plane, participants had to hold the box between their legs to reduce the distance between the box center-of-mass and their body in the initial posture in experiments. The large initial acceleration has a relatively large effect on the horizontal GRF, which is much less than the vertical GRF. However, in our optimization formulation, we imposed static initial and final conditions. This results in a difference in the horizontal GRF at initial stage when compared to the experimental data. Once this stage is passed, the trend and values of horizontal GRF are similar to the experimental data. For the other participants, the predicted joint angles also match the experimental data well, but the horizontal GRF do not, as shown in Supplemental Data.

Figure 6 depicts the predicted joint torque profiles for Participant #15. It is seen that the spine, hip, and ankle joint torques are all activated. Hip joint torque is activated for almost the entirety of the first half of the lifting time (0%–46.63% and 74.03%–82.16%). In contrast, the spine is only active for the period in middle of the lifting task (59.2%–77.0%). The ankle is active for both beginning and middle of the task (0%–2.96%, 48.85%–53.29%, and 74.02%–82.90%). Note that the dynamic joint strength curve is time-dependent, and its instantaneous value can be greater than or less than the static strength value at different times. Figure 7 shows the predicted joint torque profiles for Participant #9. It is seen that the hip (7.09%–48.94%), spine (48.23%–65.25%), and ankle (0–1.42% and 51.06%–63.83%) joint torques are activated for certain periods during the lifting process. For Participant #15, the total hip joint torque activation time period is larger than that of Participant #9 by 12.91%. The total spine activation time periods are similar between two participants (17.02% for Participant #15 and 17.08% for Participant #9), but their starting times are different. The ankle joint has different activation time periods. The spine has a similar activation history for both participants. Therefore, the kinetic lifting strategy between Participants #15 and #9 is different. In addition, Figure 8 depicts the lifting motion prediction with static joint strength for Participant #9. It is seen that the activated joint torques are bounded by static strength limits

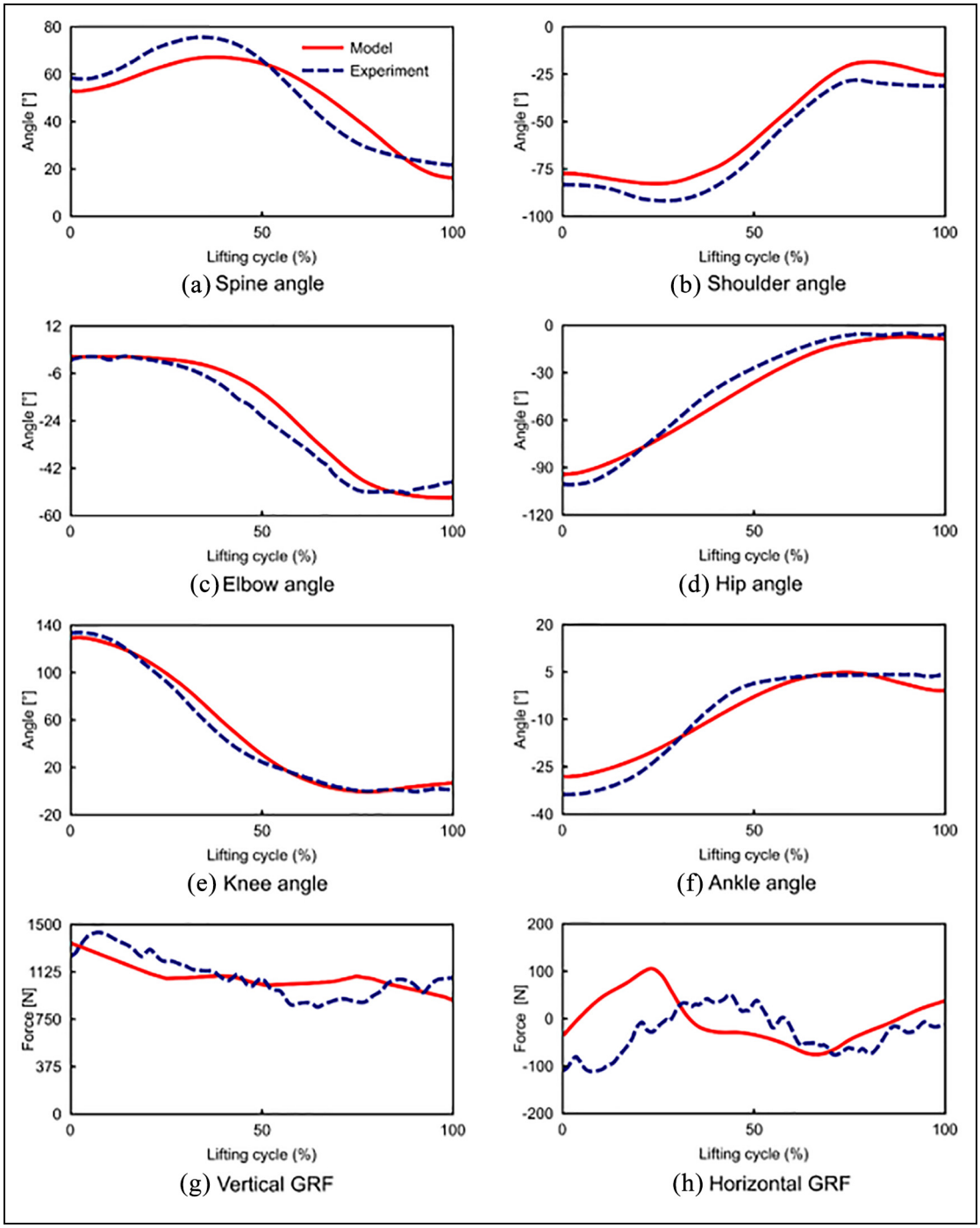

Figure 3. Kinetic and kinematic results for Participant #15.

rather than dynamic strength limits. Therefore, the predicted maximum lifting weights using static and dynamic strengths are quite different because of different torque histories.

Participants #1, #13, #17, and #18 in Figure 5 used a back-lifting strategy which is advised against by common guidelines for lifting. In this study, we did not instruct participants to use any particular strategy for maximum weight lifting—the participants each used the technique that they felt most comfortable with. They might have been able to lift a greater weight had they been trained appropriately. Since our optimization formulation imposes part of experimental postures as constraints, the maximum weight predicted corresponds to the strategy the participant used. Four cases with boundary conditions (BC) in constraint equation (20) are tested: Case 0, having zero intermediate posture constraints (only BC); Case 1, having one intermediate posture constraint at 50% time duration with BC; Case 2, having two intermediate posture constraints at 25% and 75% time duration with BC; and Case 3, having three intermediate posture constraints at 25%, 50%, and 75% time duration with BC (the default formulation in this study). Table 1 lists the

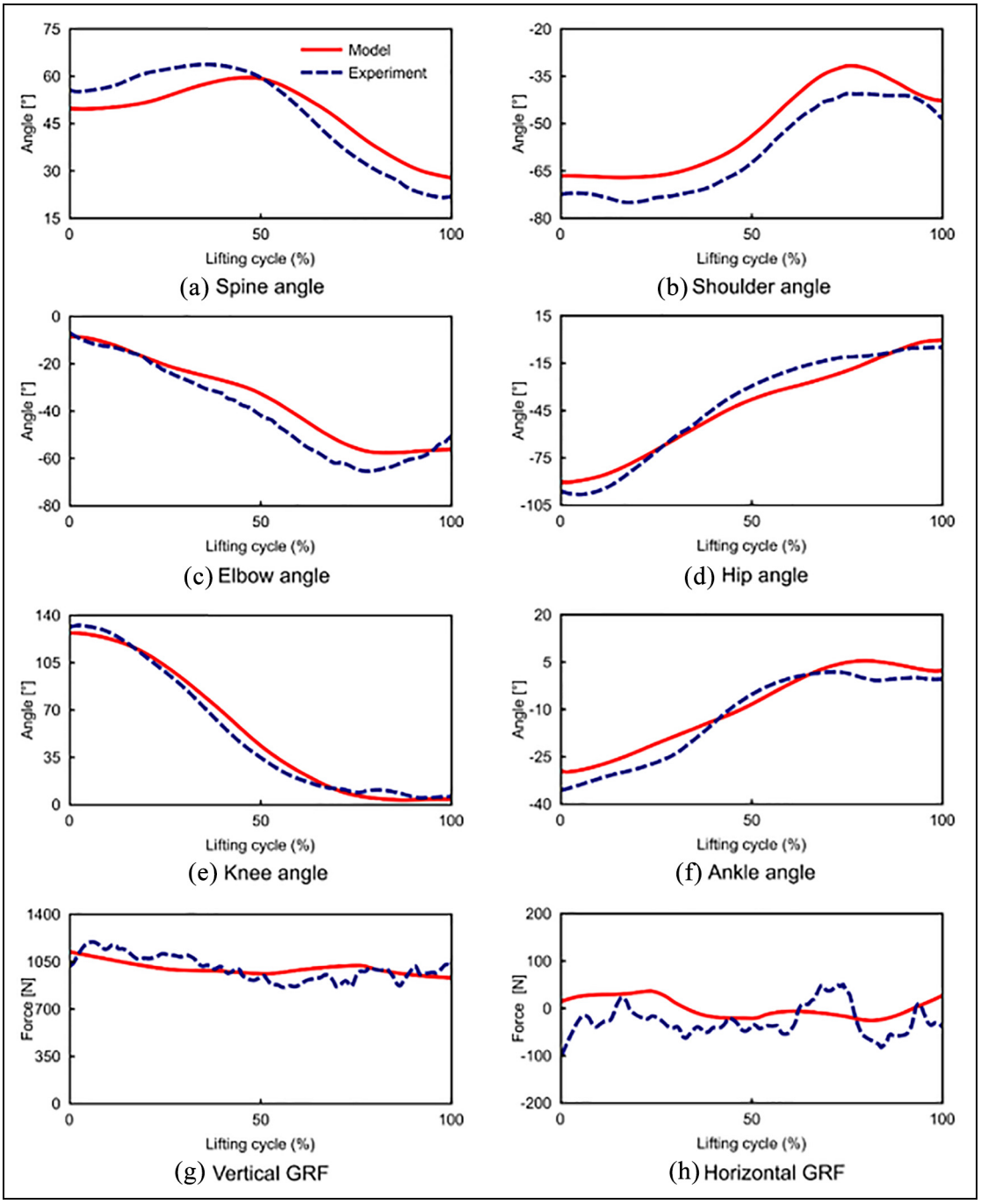

Figure 4. Kinetic and kinematic results for Participant #9.

compared results for RMSE and Pearson's correlation coefficient (r) between the predicted and the experimental results for the four cases mentioned above.

In addition, by considering Case 3, predicted box weights are compared using dynamic strength limits, static strength limits, and NIOSH equation in Table 2.

Discussion and conclusion

The major contribution of this study is to predict and validate the participant-specific maximum weight lifting considering the dynamic joint strength limits.[7] Although experimental postures were used in the optimization formulation, the optimization algorithm successfully predicts joint angles and GRF profiles, as well as box weight. Although the rationale for dynamic strength has been proposed before,[19,22] its application to lifting prediction has not been fully studied. This work is new since lifting prediction with full body dynamic strength has not been reported in previous studies.[18,20,21,24–26] In the literature, experimental methods have often been used to estimate the maximum lifting weights; however, real maximum weights cannot be obtained in a laboratory setting due to the potential for

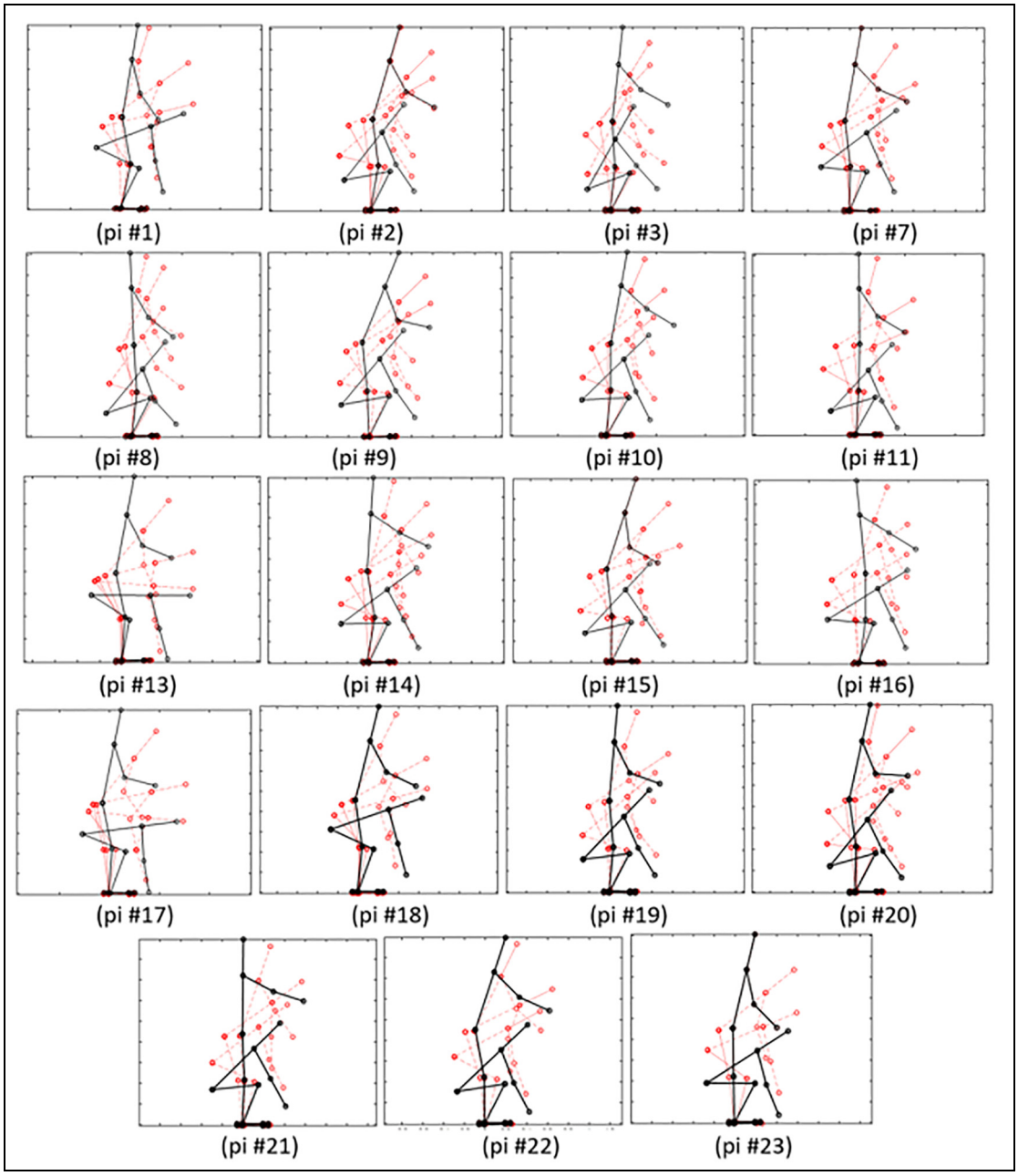

Figure 5. Snapshots of the predicted lifting motion: Participants #1, #13, #17, and #18 use a back-lifting strategy, while the other participants use the more common squat-lifting strategy (pi: participant index).

injuries.[1,8] More importantly, the current formulation sets up a foundation for future work, such as using a musculoskeletal model,[28,35] including injury risk factors, and using a multi-objective cost function including an energy term to reduce the required experimental postures in the formulation.[36] This model can be used to conduct sensitivity studies for different input parameters to predict 2D symmetric maximum weight lifting. In addition, the same optimization formulation can be applied to musculoskeletal models to study muscle biomechanics for maximum weight box lifting.

In Table 1, Case 3 has the smallest RMSE for joint angles and GRF, and Case 0 has the largest RMSE. Case 2 and Case 1 have intermediate errors. Case 1 has RMSE comparable to Case 2 for all upper body joints except the spine. For the lower body joints, Case 1 has smaller RMSE than those of Case 2. This indicates that the mid-task 50% intermediate posture constraint is important to the proposed optimization formulation. Considering Pearson's correlation coefficient (r) for the different cases, Case 3 has the largest value for joint angles and vertical GRF, which indicates Case 3 is a more accurate model. For upper body joints, r-values for Cases 0, 1, and 2 are similar. For lower body joints, r-values decrease following the order of Case 3, 1, 2, and 0. It is noted the vertical GRF have a smaller r-value than that for the joint angles, because no intermediate force constraints are imposed on GRF—only

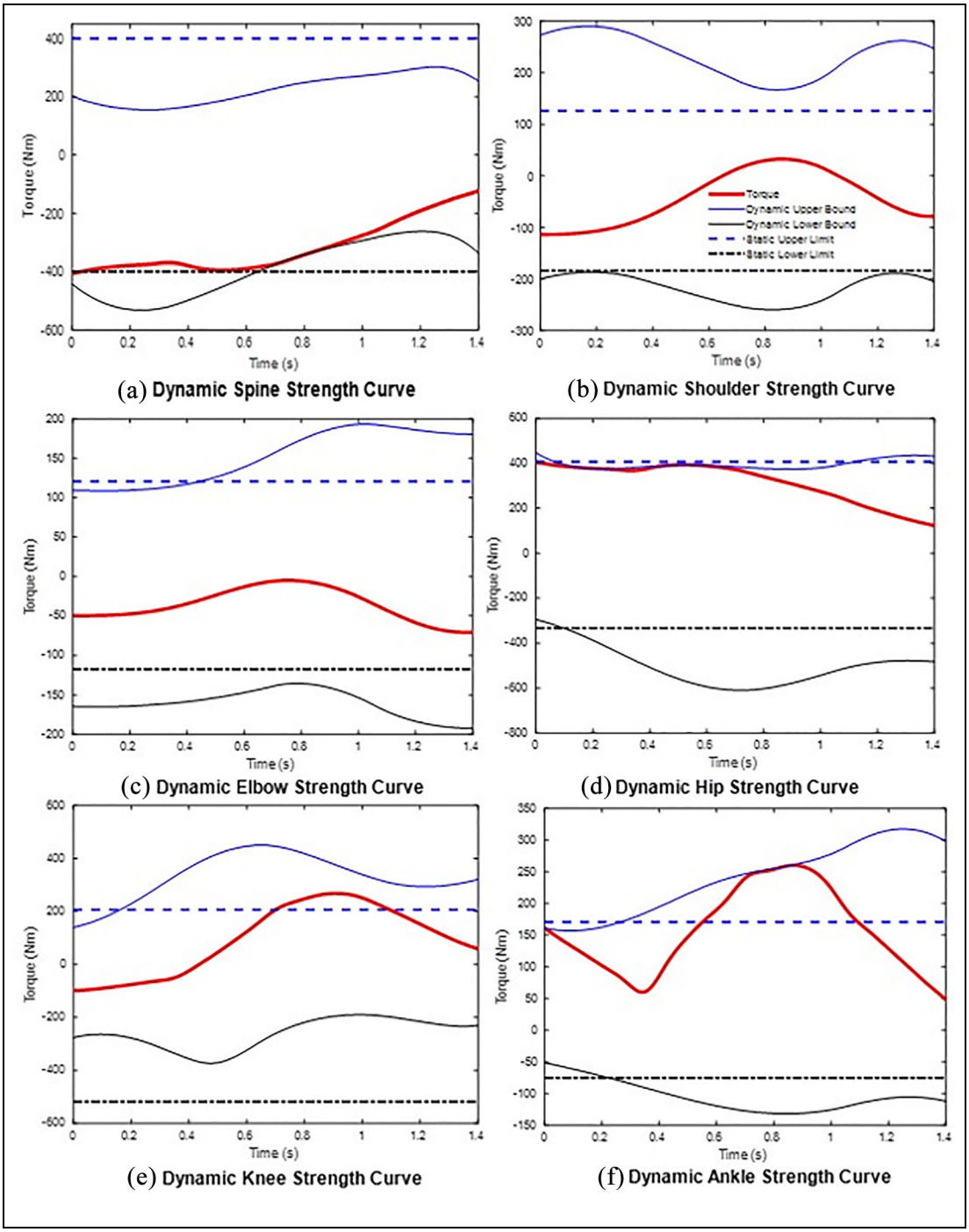

Figure 6. Joint torque profiles for Participant #15 using dynamic joint strength limits.

intermediate posture (joint angle) constraints are used. For horizontal GRF, r is negative, indicating that the predicted average horizontal GRF and the experimental value have different directions. This is because the large initial impact acceleration applied to the box directed toward the center-of-mass of the participant for the maximum weight lifting as observed in the experiment has not been considered in the simulation formulation. It is concluded that imposing postural constraints—especially the boundary and mid-time constraints—from experiments is important to accurately predict kinetics and kinematics. This observation is consistent with the findings in the literature.[21,37]

It is interesting to note that the elbow correlations for all constraints are low, as seen in Table 1. The elbow joint has the most widely varying strategy among participants when compared to other joints in the experiment. The maximum weight lifting requires the participant to lift the box to reach the final position on a table. The participants have different strengths at the elbow joint, so their elbow kinematics for the lifting and the reach motions are very different. Therefore, we

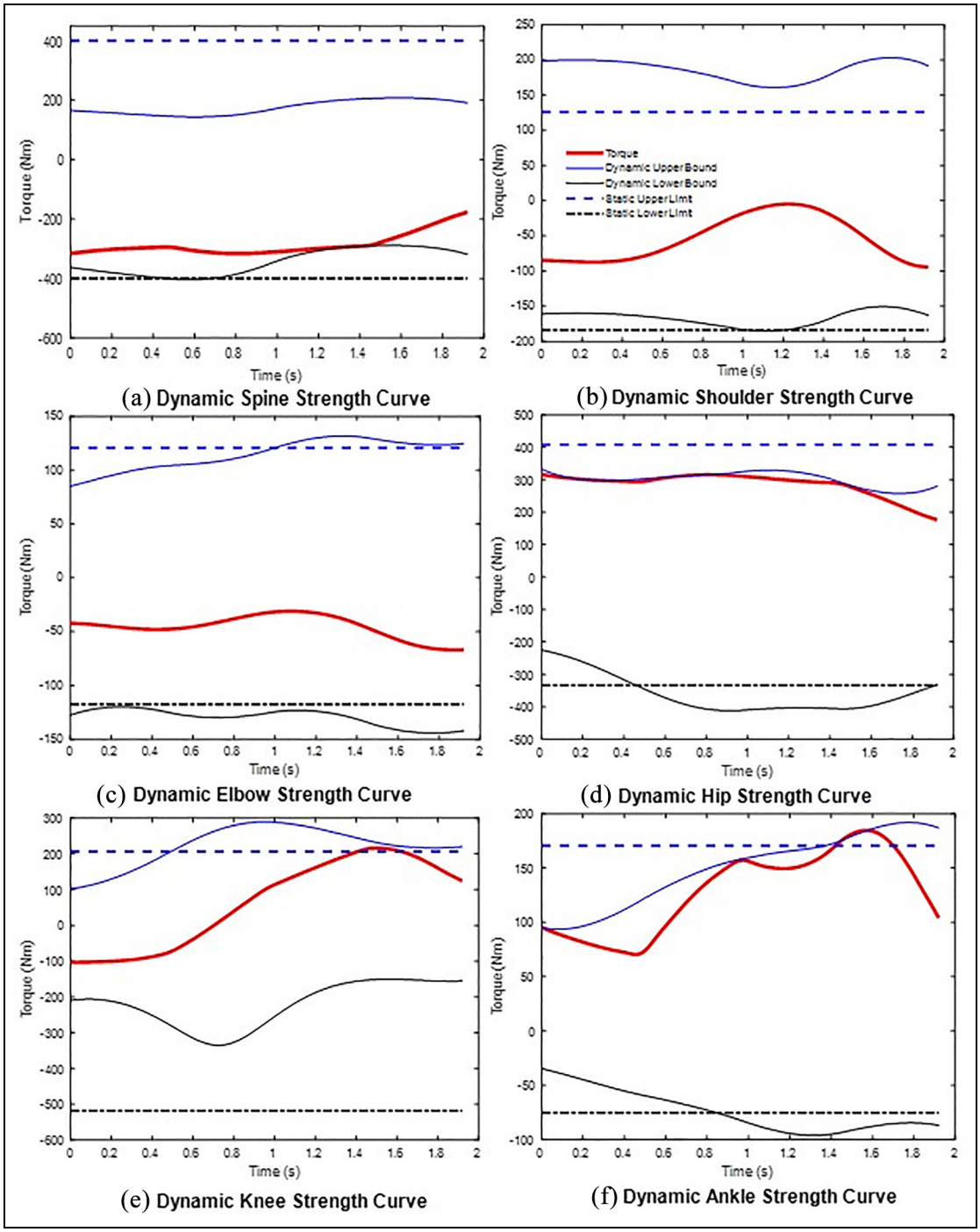

Figure 7. Joint torque profiles for Participant #9 using dynamic joint strength limits.

need to impose more intermediate constraints to improve the elbow correlations. This is a new finding for maximum weight-lifting prediction.

In Table 2, the predicted box weights considering dynamic joint strength are close to the experimental box weights. This demonstrates that the proposed maximum weight optimization formulation and the enumeration-based participant-specific strength retrieval approach work well. Note that in this study, three intermediate posture constraints (Case 3) were used for z_score calculations, but our previous study[7] used only a single intermediate posture constraint. The more intermediate posture constraints are used, the more accurate the z_score. The participant-specific dynamic joint strength is the major limiting factor for maximum weight-lifting prediction. The prediction is sensitive to the strength limit constraints—as seen in Table 2, the predicted weights using static strength limits are different from those using dynamic joint strength. This further demonstrates that dynamic strength is required to predict maximum lifting weight. The static strength predicts larger box weights for all participants except

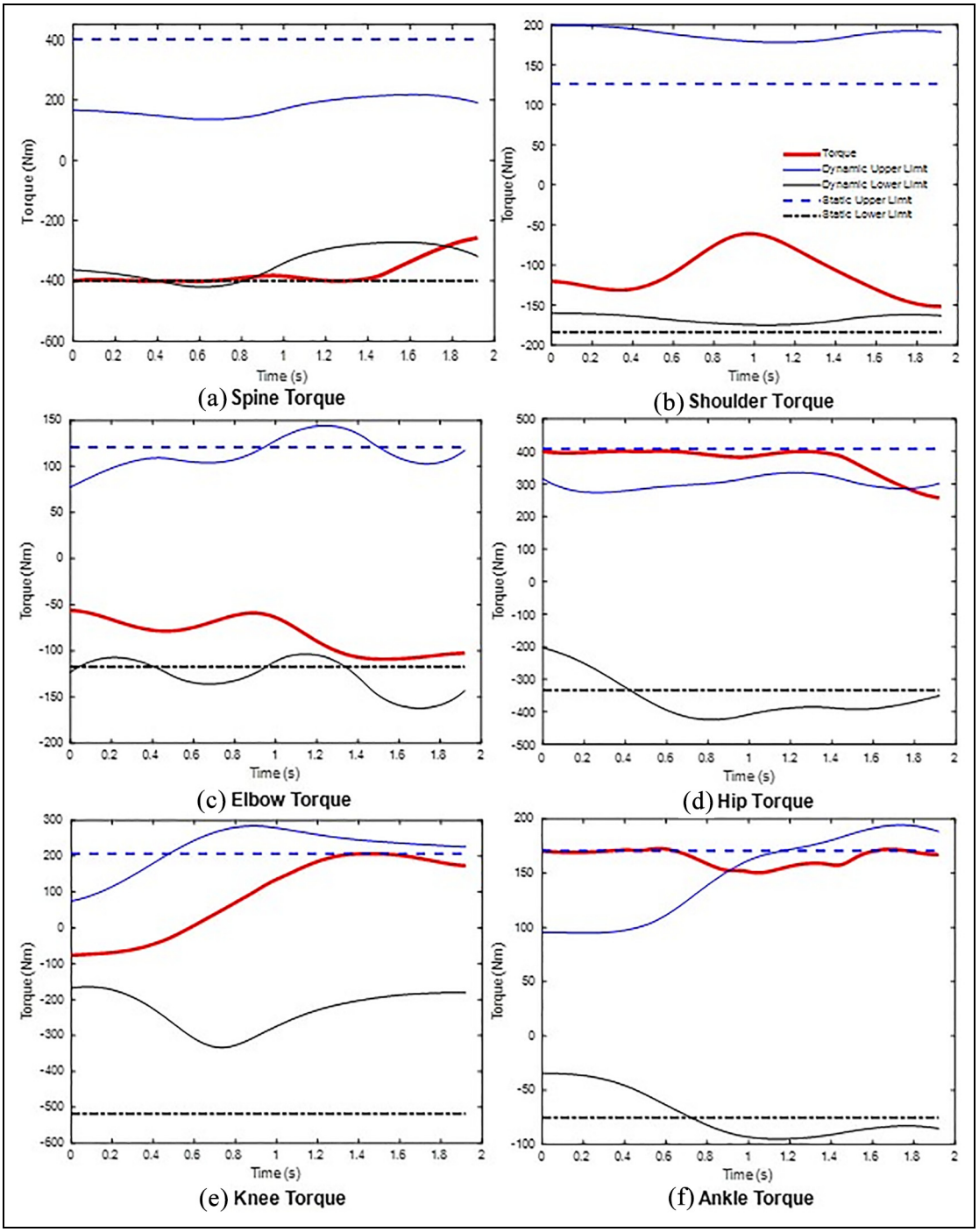

Figure 8. Joint torque profiles for Participant #9 using static joint strength limits.

Participant #1. From this interesting finding, we may recognize that Participant #1 is an exceptionally strong person who can lift more weight under dynamic strength limits than under the given static strength. We also compared our predicted box weights with NIOSH equation results which yields much smaller weights than our method considering dynamic joint strength. This is because NIOSH equation considers lifting frequency and working hours. The input parameters for NIOSH equation in Table 1 include box horizontal locations, box vertical locations, 0.2 lifts/min frequency, 1-h working duration, and good coupling conditions. In contrast, our prediction is a one-time maximum weight lifting without any fatigue. Muscle motor fatigue is governed by ordinary differential equations[38–40] which are not included in the current simulation model. In the future, we will develop a lifting model considering muscle fatigue for repetitive lifting prediction.

There are some limitations to our approach. First, five lifting postures from experiments are imposed as constraints in the optimization formulation. This

Table 1. Accuracy metrics averaged across 16 participants for prediction of joint angle and GRF profiles by simulations with 0, 1, 2, and 3 intermediate posture constraints from experiments.

	Case 0:0 intermediate constraint[a]		Case 1:1 intermediate constraint		Case 2:2 intermediate constraints		Case 3:3 intermediate constraints	
	RMSE	*r*	RMSE	*r*	RMSE	*r*	RMSE	*r*
Spine	15.61 (2.52)	0.86 (0.10)	14.08 (2.31)	0.77 (0.17)	7.34 (0.72)	0.95 (0.04)	7.03 (0.45)	0.96 (0.02)
Shoulder	16.83 (6.82)	0.90 (0.06)	14.29 (5.43)	0.88 (0.10)	13.27 (4.01)	0.88 (0.09)	6.82 (1.12)	0.98 (0.02)
Elbow	38.64 (9.92)	0.59 (0.31)	23.17 (11.49)	0.30 (0.59)	22.36 (8.58)	0.57 (0.31)	6.62 (1.74)	0.71 (0.46)
Hip	27.31 (13.08)	0.81 (0.10)	8.16 (1.43)	0.97 (0.03)	14.06 (4.89)	0.92 (0.05)	6.88 (0.96)	0.98 (0.02)
Knee	44.34 (19.13)	0.76 (0.13)	12.29 (4.62)	0.95 (0.06)	21.92 (9.66)	0.86 (0.14)	6.60 (1.39)	0.98 (0.02)
Ankle	13.84 (4.81)	0.53 (0.28)	5.33 (2.04)	0.92 (0.09)	8.50 (2.84)	0.73 (0.21)	3.81 (1.21)	0.96 (0.04)
Vertical GRF[b]	154.01 (48.46)	0.02 (0.23)	116.01 (39.25)	0.30 (0.31)	114.89 (27.13)	0.30 (0.32)	93.24 (20.30)	0.57 (0.20)
Horizontal GRF[b]	54.64 (14.09)	–0.19 (0.32)	56.09 (15.62)	–0.18 (0.34)	51.01 (12.26)	–0.08 (0.36)	51.41 (13.41)	–0.15 (0.36)

GRF: ground reaction forces; RMSE: root-mean-square error.All values of root-mean-square error (RMSE) and Pearson's correlation coefficient (*r*) are represented as mean (standard deviation).

Note that Participants #8, #11, and #17 did not converge for certain intermediate constraints, so they are excluded from the analysis.

[a]Boundary conditions with 0 intermediate posture constraints; with 1 intermediate posture constraint at 50% time duration; with 2 intermediate posture constraints at 25% and 75% time duration; and with 3 intermediate posture constraints at 25%, 50%, and 75% time duration.

[b]RMSE values are in Newton, and all other parameters are in degrees.

Table 2. Predicted box weights using dynamic joint strength, static strength, and NIOSH equation.

Participant index	Time (s)	z_score	Experiment weight (N)	Weight 1[a] (N)	Weight 2[b] (N)	NIOSH weight (N)
1	1.36	1.86	343.98	358.13	194.68	90.16
2	1.65	0.53	233.73	238.43	360.39	92.12
3	1.77	–0.02	189.63	202.34	418.98	88.20
7	1.80	0.43	255.78	263.36	326.17	81.34
8	1.44	1.05	233.73	237.65	316.98	92.12
9	1.93	0.33	211.68	218.39	344.44	87.22
10	1.55	0.84	233.73	250.17	255.07	86.24
11	1.41	1.55	233.73	226.24	248.83	75.46
13	1.54	–0.22	145.53	150.75	390.59	88.20
14	2.17	0.65	233.73	239.14	252.11	71.54
15	1.41	1.07	255.78	262.89	274.17	71.54
16	1.59	0.59	233.73	237.94	284.34	79.38
17	2.06	0.53	211.68	213.33	291.17	83.30
18	1.57	0.38	145.53	157.87	240.93	79.38
19	1.57	0.14	167.58	178.44	351.12	98.00
20	2.40	0.43	211.68	246.55	365.67	79.38
21	1.70	0.56	211.68	221.82	317.77	85.26
22	1.36	0.76	211.68	229.84	295.88	81.34
23	1.21	1.10	277.83	284.40	293.42	98.98

NIOSH: National Institute for Occupational Safety and Health.

[a]Weight 1 is the prediction using dynamic joint strength with three intermediate constraints.

[b]Weight 2 is the prediction using static joint strength with three intermediate constraints.

reduces the flexibility of the optimization prediction, that is, there is a tradeoff between the power of prediction and the accuracy of the predicted result.[37] Second, only the box weight is considered in the objective function, and no energy term is included. Finally, there are potential inaccuracies in the dynamic joint strength database from the literature.[2–6] It is noted that we cannot test 100% (maximum) lifting weight experimentally, and the same limitation affects the joint strength database, all of whose data were also obtained under the safe-maximum-strength condition.

Future work should include the following: (1) extending the 2D prediction method to the 3D case to study asymmetric box-lifting tasks; (2) validating the 3D prediction method through experiments; (3) extending the skeletal model to a musculoskeletal model; (4) including a fatigue model in the box-lifting simulation; and (5) a sensitivity analysis of parameters that result in box-lifting injuries so that regulations can be developed to reduce injuries for workers.

Acknowledgements

The authors appreciate all the anonymous reviewers for their time and constructive criticism to improve the quality of this paper.

Declaration of conflicting interests

The author(s) declared no potential conflicts of interest with respect to the research, authorship, and/or publication of this article.

Funding

The author(s) disclosed receipt of the following financial support for the research, authorship, and/or publication of this article: This work was supported by the National Science Foundation (grant nos CBET 1849279 and 1703093) and the Honors College, Texas Tech University.

Supplemental material

Supplemental material for this article is available online.

ORCID iD

Yujiang Xiang https://orcid.org/0000-0003-0866-2802

References

1. Waters T, Putz-Anderson V and Garg A. *Quick guide for the NIOSH lifting equation*. Cincinnati, OH: DHHS Publication, 1994.
2. Khalaf KA, Parnianpour M, Sparto PJ, et al. Modeling of functional trunk muscle performance: interfacing ergonomics and spine rehabilitation in response to the ADA. *J Rehabil Res Dev* 1997; 34(4): 459–469.
3. Azghani MR, Farahmand F, Meghdari A, et al. Design and evaluation of a novel triaxial isometric trunk muscle strength measurement system. *Proc IMechE, Part H: J Engineering in Medicine* 2009; 223(6): 755–766.
4. Frey-Law LA, Laake A, Avin KG, et al. Knee and elbow 3D strength surfaces: peak torque-angle-velocity relationships. *J Appl Biomech* 2012; 28(6): 726–737.
5. Looft JM. *Adaptation and validation of an analytical localized muscle fatigue model for workplace tasks*. PhD Thesis, Department of Biomedical Engineering, The University of Iowa, Iowa City, IA, 2014.
6. Hussain SJ and Frey-Law LA. 3D strength surfaces for ankle plantar- and dorsi-flexion in healthy adults: an isometric and isokinetic dynamometry study. *J Foot Ankle Res* 2016; 9: 43.
7. Xiang Y, Zaman R, Rakshit R, et al. Subject-specific strength percentile determination for two-dimensional symmetric lifting considering dynamic joint strength. *Multibody Syst Dyn* 2019; 46(1): 63–76.
8. Freivalds A, Chaffin DB, Garg A, et al. A dynamic biomechanical evaluation of lifting maximum acceptable loads. *J Biomech* 1984; 17(4): 251–262.
9. Davy DT and Audu ML. A dynamic optimization technique for predicting muscle forces in the swing phase of gait. *J Biomech* 1987; 20(2): 187–201.
10. Farahani SD, Andersen MS, de Zee M, et al. Optimization-based dynamic prediction of kinematic and kinetic patterns for a human vertical jump from a squatting position. *Multibody Syst Dyn* 2016; 36(1): 37–65.
11. Xiang Y, Arora JS and Abdel-Malek K. Optimization-based prediction of asymmetric human gait. *J Biomech* 2011; 44(4): 683–693.
12. De Groote F, Kinney AL, Rao AV, et al. Evaluation of direct collocation optimal control problem formulations for solving the muscle redundancy problem. *Ann Biomed Eng* 2016; 44: 2922–2236.
13. Ackermann M and van den Bogert AJ. Optimality principles for model-based prediction of human gait. *J Biomech* 2010; 43(6): 1055–1060.
14. Thelen DG and Anderson FC. Using computed muscle control to generate forward dynamic simulations of human walking from experimental data. *J Biomech* 2006; 39(6): 1107–1115.
15. Shourijeh MS, Smale KB, Potvin BM, et al. A forward-muscular inverse-skeletal dynamics framework for human musculoskeletal simulations. *J Biomech* 2016; 49: 1718–1723.
16. Yamasaki T, Idehara K and Xin X. Estimation of muscle activity using higher-order derivatives, static optimization, and forward-inverse dynamics. *J Biomech* 2016; 49: 2015–2022.
17. Ayoub MM. Problems and solutions in manual materials handling: the state of the art. *Ergonomics* 1992; 35(7–8): 713–728.
18. Hsiang SM and Ayoub MM. Development of methodology in biomechanical simulation of manual lifting. *Int J Ind Ergonom* 1994; 13: 271–288.
19. Aghazadeh F and Ayoub MM. A comparison of dynamic- and static-strength models for prediction of lifting capacity. *Ergonomics* 1985; 28(10): 1409–1417.
20. Chang CC, Brown DR, Bloswick DS, et al. Biomechanical simulation of manual lifting using space-time optimization. *J Biomech* 2001; 34(4): 527–532.
21. Chang CC, McGorry RW, Lin JH, et al. Prediction accuracy in estimating joint angle trajectories using a video posture coding method for sagittal lifting tasks. *Ergonomics* 2001; 53(8): 1039–1047.
22. Gündogdu Ö, Anderson KS and Parnianpour M. Simulation of manual materials handling: biomechanical assessment under different lifting conditions. *Technol Health Care* 2005; 13(1): 57–66.
23. Xiang Y. An inverse dynamics optimization formulation with recursive B-spline derivatives and partition of unity contacts: demonstration using two-dimensional musculoskeletal arm and gait. *J Biomech Eng* 2019; 141(3): 034503.
24. Eriksson A and Nordmark A. Temporal finite element formulation of optimal control in mechanisms. *Comput Method Appl M* 2010; 199: 1783–1792.
25. Huang C, Sheth PN and Granata KP. Multibody dynamics integrated with muscle models and space-time constraints for optimization of lifting movements. In: *Proceedings of the ASME international design engineering technical conferences*, Long Beach, CA, 24–28 September 2005, pp.391–398. New York: ASME.
26. Song J, Qu X and Chen CH. Simulation of lifting motions using a novel multi-objective optimization approach. *Int J Ind Ergonom* 2016; 53: 37–47.
27. Xiang Y and Arefeen A. Computational methods for skeletal muscle strain injury: a review. *Crit Rev Biomed Eng* 2019; 47(4): 277–294.
28. Schultz AB, Anderson BJ, Haderspeck K, et al. Analysis and measurement of lumber trunk loads in tasks involving bends and twists. *J Biomech* 1982; 15(9): 669–675.
29. Denavit J and Hartenberg RS. A kinematic notation for lower-pair mechanisms based on matrices. *ASME J Appl Mech* 1955; 22: 215–221.
30. Xiang Y, Arora JS and Abdel-Malek K. Optimization-based motion prediction of mechanical systems: sensitivity analysis. *Struct Multidiscip O* 2009; 37(6): 595–608.

31. VICON. Plug-in gait reference guide, https://docs.vicon.com/display/Nexus25/Plug-in+Gait+Reference+Guide (accessed 12 December 2019).
32. Cloutier A, Boothby R and Yang J. Motion capture experiments for validating optimization-based human models. In: *Proceedings of the HCI international, 3rd international conference on digital human modelling*, Orlando, FL, 9–14 July 2011, pp.59–68. Berlin: Springer.
33. Mital A and Kromodihardjo S. Kinetic analysis of manual lifting activities: part II—biomechanical analysis of task variables. *Int J Ind Ergonom* 1986; 1: 91–101.
34. Cheng H, Obergefell L and Rizer A. *Generator of body data (GEBOD) manual*. Technical report no. AL.CF-TR-1994-0051, March 1994. Dayton, OH: Armstrong Laboratory, Wright-Patterson Air Force Base.
35. Christophy M, Senan NAF, Lotz JC, et al. A musculoskeletal model for the lumbar spine. *Biomech Model Mechan* 2012; 11(1–2): 19–34.
36. Xiang Y, Cruz J, Zaman R, et al. Multi-objective optimization for two-dimensional maximum weight lifting prediction considering dynamic strength. *Eng Optimiz*. Epub ahead of print 10 January 2020. DOI: 10.1080/0305215X.2019.1702979.
37. Xiang Y, Chung HJ, Kim JH, et al. Predictive dynamics: an optimization-based novel approach for human motion simulation. *Struct Multidiscip O* 2010; 41: 465–479.
38. Xia T and Frey-Law LA. A theoretical approach for modeling peripheral muscle fatigue and recovery. *J Biomech* 2008; 41: 3046–3052.
39. Looft JM, Herkert N and Frey-Law LA. Modification of a three-compartment muscle fatigue model to predict peak torque decline during intermittent tasks. *J Biomech* 2018; 77: 16–25.
40. Rakshit R and Yang J. Modelling muscle recovery from a fatigued state in isometric contractions for the ankle joint. *J Biomech* 2020; 100: 109601.